Electron paramagnetic resonance and other allied studies of sol–gel derived nanocrystalline chromium oxides in a silica glass matrix

2005 J. Phys.: Condens. Matter 17 3385

(http://iopscience.iop.org/0953-8984/17/21/031)

INSTITUTE OF PHYSICS PUBLISHING JOURNAL OF PHYSICS: CONDENSED MATTER

J. Phys.: Condens. Matter **17** (2005) 3385–3403 doi:10.1088/0953-8984/17/21/031

Electron paramagnetic resonance and other allied studies of sol–gel derived nanocrystalline chromium oxides in a silica glass matrix

Sudip Mukherjee[1], **A K Pal**[1] **and S Bhattacharya**[2,3]

[1] Department of Solid State Physics, Indian Association for the Cultivation of Science, Jadavpur, Kolkata-700 032, India
[2] Wihuri Physical Laboratory, Department of Physics, University of Turku, Turku-20014, Finland
[3] Department of Physics, Åbo Akademi University, Turku-20500, Finland

E-mail: sspsm3@mahendra.iacs.res.in (S Mukherjee)

Received 4 March 2004, in final form 21 March 2005
Published 13 May 2005
Online at stacks.iop.org/JPhysCM/17/3385

Abstract

Monolithic silica gels doped with various concentrations (1, 5, 10 mol%) of chromium oxide are prepared by a sol–gel process and are subjected to calcination at different temperatures up to 1200 °C. This has principally led to the formation of Cr_2O_3 nanocrystals and also of CrO_3 nanocrystals at the higher calcination temperatures. The sizes of the Cr_2O_3 nanocrystals have been determined by x-ray diffraction (XRD) and transmission electron microscopy (TEM) studies and have been found to lie in the range 5–30 nm depending upon the dopant concentration as well as the calcination temperature. The formation of nonmagnetic CrO_3 crystals in 10 mol% chromium oxide doped silica glass calcined at 1200 °C as a result of oxidation of Cr^{5+} ions to Cr^{6+} ions has been confirmed from XRD studies. Optical, infrared and X-band electron paramagnetic resonance (EPR) spectra of these nanocrystals have also been studied. EPR behaviours such as the g-factor and linewidth of Cr_2O_3 nanocrystals investigated at room and liquid nitrogen temperatures have been found to be quite distinct from those of antiferromagnetic (AF) bulk Cr_2O_3 crystals and may be manifestations of superparamagnetism/ferromagnetism in these nanocrystals. A narrow anisotropic EPR line ($g_\parallel = 1.955$; $g_\perp = 1.976$) has been detected for chromium oxide doped silica gel calcined at 800 °C and has been assigned to isolated Cr^{5+} ions in a tetragonally distorted tetrahedral environment. Studies of the thermal dependence of zero-field-cooled (ZFC) and field-cooled (FC) magnetization (σ) 10 mol% chromium oxide doped silica glasses calcined at 800 °C by a SQUID magnetometer in the 5–300 K temperature range have revealed the occurrence of the blocking temperature T_B at about 250 K, which is a characteristic feature of superparamagnetism in Cr_2O_3 nanocrystals. The superparamagnetic effects are almost quenched in the samples calcined at 1000 and 1200 °C because of the presence of larger

nanocrystals in these samples. Magnetic hysteresis effects in these calcined samples at 300 K as well as at 5 K in the ±6 T magnetic field range have also been investigated. The existence of ferromagnetic order at low temperature (5 K) as well as at room temperature (300 K) (for samples calcined at higher temperatures) has been confirmed.

1. Introduction

In recent times, various physical properties of transition metal oxide particles including magnetism in the nanometre regime have been the object of great interest, and they have been investigated both experimentally [1, 2] and theoretically [3–5]. Some magnetic nanoparticles embedded in glass or polymer matrices have revealed superparamagnetism as well as a number of other properties having the potential of technical applications [6]. Superparamagnetism is a phenomenon by which nanosized magnetic materials may exhibit a behaviour similar to paramagnetism at temperatures below the Curie or the Néel temperature, except that instead of each individual atom being independently influenced by an external magnetic field, the magnetic moment of the entire nanoparticle tends to align with the magnetic field. Nanosized Fe_2O_3 (hematite) particles prepared by heating ferric nitrate and subjected to neutron scattering experiments have displayed superparamagnetic relaxation and precession modes [7]. The superparamagnetic behaviours of $MgFe_2O_4$ spinel ferrite nanocrystals such as the blocking temperature and coercivity unambiguously correlate with the particle size [8]. Magnetization experiments on highly concentrated Fe_2O_3 nanoparticles in an alumina matrix (68% Fe_2O_3 in weight) have indicated a superparamagnetic behaviour of interacting particles, the zero-field-cooled susceptibility showing a maximum at $T \cong 145$ K [9]. Computer simulation electron paramagnetic resonance (EPR) studies of annealed iron containing borate glass have been very useful in understanding the morphology of magnetic nanomaterials [10]. Structural, magnetic and Mössbauer properties of Fe_2O_3 nanoparticles prepared by the pulsed wire method have been studied [11]. A quadruple line at the centre of the Mössbauer spectrum represents the superparamagnetic phase of γ-Fe_2O_3 with a mean particle size of 7 nm and below. NiO nanoparticles prepared by the calcination of chemically precipitated $Ni(OH)_2$ at various temperatures, unlike bulk NiO antiferromagnetism, have exhibited anomalous magnetic properties such as large moments and coercivities and loop shifts [12]. The magnetization of CuO nanoparticles synthesized by a sol–gel process in combination with high temperature annealing was studied in the temperature range 5–350 K [13]. CuO nanoparticles below 10 nm have exhibited magnetism with uncompensated surface spins resulting in a weak ferromagnetic component, and those greater than 10 nm have displayed magnetic ordering which is essentially similar to the antiferromagnetic ordering of the bulk CuO but with a reduced T_N. Nanosized Cr_2O_3 particles have been produced by various methods. One such method of synthesis is by gas condensation followed by *in situ* consolidation. The nanophase powder has demonstrated characteristic superparamagnetic behaviour in both its powder and consolidated forms [14], although bulk Cr_2O_3 is known to be antiferromagnetic [15]. Synthesis of nanocrystalline Cr_2O_3 particles was also performed in a microwave plasma using chromium hexacarbonyl as precursor, and its magnetic behaviour in the temperature range 10–300 K has been described by a modified Langevin function with the magnetic moment having a thermally activated component [16].

The sol–gel method of preparation of inorganic oxide glasses has many advantages over the traditional melt processing techniques in that greater homogeneity and purity can be attained

as well as lower processing temperatures and better control over the glass properties. The properties of silica (SiO_2) glass prepared by a sol–gel process have been extensively studied in recent times. It has been found that silica gel becomes porous glass when calcined at ∼400 °C and that the collapse of pores takes place at ∼700 °C and becomes nearly complete at ∼800 °C [17]. So, when silica gels doped with various concentrations of transition metal ions are prepared, there is a possibility that the collapse of the silica pores taking place near 700 °C will trigger isolated metal ions to come close together to form clusters which may have dimensions in the nanometre range (nanoparticles). With the primary objective of understanding the clustering phenomenon, particularly reflected in the EPR properties of the transition metal oxide nanoparticles, preparation of silica gels and glasses doped with transition metal ions, namely, chromium metal ions in various concentrations obtained via a sol–gel route, and their characterization by EPR, infrared (IR), optical absorption, x-ray diffraction (XRD), and transmission electron microscopy (TEM) have been undertaken. Zero-field-cooled (ZFC) and field-cooled (FC) magnetization and magnetic hysteresis studies have also been carried out in the temperature range 5–300 K. In the present communication, the results of such investigations on 1.0, 5.0 and 10 mol% Cr-doped SiO_2 gel–glass heat treated at various temperatures up to 1200 °C are reported. A preliminary report was presented at the DAE Solid State Physics Symposium held at Chandigarh, India, 25–31 December 2002.

2. Experimental details

Chromium oxide doped silica gel was prepared from silicon tetraethylorthosilicate (TEOS) and dopant chromium nitrate nonahydrate having various mol% concentrations, namely, 1.0 (Cr1), 5.0 (Cr5) and 10.0 (Cr10) mol%, essentially following the method of Sakka and Kamiya [18]. The molar ratio of water and TEOS was kept at 20, and that of TEOS and catalyst HCl at 100. Dry ethanol was used as solvent. The solution, poured in a Pyrex beaker and covered with a polythene sheet, was kept in the atmosphere for 7–8 days to form a stiff monolithic gel. The monolithic gels were then allowed to dry further at room temperature for 4–5 weeks. The dried gels were then transferred to a furnace. Heat treatments of these samples were then performed in air at several pre-selected temperatures up to 1200 °C, in accordance with the following schedule [19]:

$$\begin{aligned}\mathrm{RT} &\xrightarrow{3.5\ \mathrm{h}} 250\,^{\circ}\mathrm{C}\ (4\ \mathrm{h}) \xrightarrow{2.5\ \mathrm{h}} 310\,^{\circ}\mathrm{C}\ (4\ \mathrm{h}) \xrightarrow{2.5\ \mathrm{h}} 440\,^{\circ}\mathrm{C}\ (16\ \mathrm{h}) \xrightarrow{2.5\ \mathrm{h}} 500\,^{\circ}\mathrm{C}\ (4\ \mathrm{h})\\ &\xrightarrow{2.5\ \mathrm{h}} 600\,^{\circ}\mathrm{C}\ (4\ \mathrm{h}) \xrightarrow{2.5\ \mathrm{h}} 700\,^{\circ}\mathrm{C}\ (4\ \mathrm{h}) \xrightarrow{2.5\ \mathrm{h}} 800\,^{\circ}\mathrm{C}\ (4\ \mathrm{h}) \xrightarrow{2.5\ \mathrm{h}} 900\,^{\circ}\mathrm{C}\ (4\ \mathrm{h})\\ &\xrightarrow{1.5\ \mathrm{h}} 950\,^{\circ}\mathrm{C}\ (4\ \mathrm{h}) \xrightarrow{1.5\ \mathrm{h}} 1000\,^{\circ}\mathrm{C}\ (4\ \mathrm{h}) \xrightarrow{2.5\ \mathrm{h}} 1200\,^{\circ}\mathrm{C}\ (4\ \mathrm{h}).\end{aligned}$$

The gel–glasses were removed from the furnace at pre-selected temperatures and stored inside a oven maintained at 130 °C.

EPR spectra of Cr10, Cr5 and Cr1 samples calcined at 500, 700, 800, 900, 1000, 1200 °C were recorded in a Varian X-band EPR spectrometer (Model E-109) with 100 kHz magnetic field modulation at room (RT) and liquid nitrogen (LNT) temperatures. Powder XRD of Cr1 and Cr10 glass specimens calcined at the respective temperatures of 800, 1000 °C and 800, 1000, 1200 °C were recorded using a Seifert diffractometer (Model: XRD3000) with Cu Kα radiation as source. With the help of a Hitachi transmission electron microscope (Model: H600) TEM was carried out only on Cr10 glass samples in fine glass powder form sprinkled on carbon grids. The IR spectra of KBr emulsion of the samples having thicknesses in the range 0.1–0.3 mm are also recorded using an IR Nicolet spectrometer (Model: MAGNA-IR750 series II) in the range 4000–400 cm^{-1}. Optical absorption spectra of Cr1 sample calcined at 800 °C were recorded in the 200–2500 nm range with the help of an IR–vis Hitachi

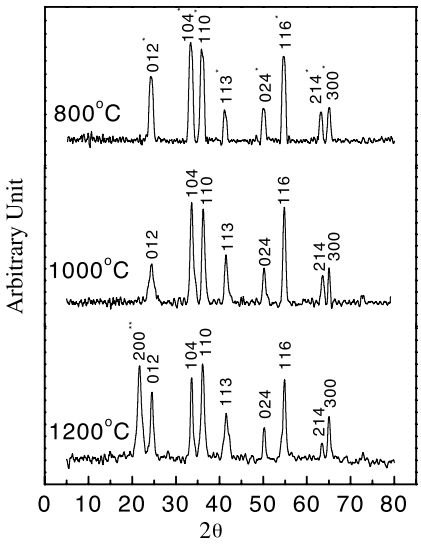

Figure 1. XRD lines of Cr10 silica glass calcined at 800, 1000 and 1200 °C. *:Cr_2O_3 crystal; **:CrO_3 crystal.

spectrometer (Model: U-3410). Thereafter the above spectrometer unfortunately became out of order, and so the absorption spectral measurements for Cr1 samples in the gel form and calcined at 500 °C were carried out with the help of a Shimadzu UV–vis spectrometer (Model: 2101PC) in the 200–900 nm region. The magnetization and magnetic hysteresis measurements were performed on a Cryogenics S600 superconducting quantum interface device (rf-SQUID magnetometer) with temperature varying from 5 to 300 K with ±1.0 K thermal stability, equipped with a superconducting magnet producing fields up to ±6 T. To perform these measurements, the sample in the powder form was packed in a pocket made from PTFE tape and fixed to a length of copper wire. Masses of the samples were chosen in the range 8–12 mg to obtain a good signal-to-noise ratio. Cr10 samples calcined at 800, 1000 and 1200 °C were first cooled in zero magnetic field down to 5 K and then magnetizations were recorded by increasing the temperature in an applied magnetic field (200 Oe) (ZFC measurements). FC curves were recorded by cooling the samples again in the presence of the same field. To obtain the field dependence of the magnetization, i.e., hysteresis loop, the samples were cooled to a specific temperature and then the sample's magnetic moment as a function of field was recorded in the magnetic field range of ±6 T. These experiments were performed at three temperatures: 5, 100 and 300 K.

3. Results and discussions

3.1. XRD spectra

Powder XRD in the domain $2\theta = 5°$–$80°$ has shown that Cr1 glass calcined at 800 °C is amorphous. At higher calcined temperature, (1000 °C), the glass is predominantly amorphous. Only a very feeble (104) line, due to Cr_2O_3 nanocrystals, can be traced with great difficulty in the XRD domain, $2\theta = 5°$–$80°$. The x-ray diffraction lines of Cr10 glass (figure 1) calcined at 800 °C have clearly indicated the presence of the crystalline phase of Cr_2O_3. XRD of glasses calcined at 1000 and 1200 °C has revealed that the lines belonging to Cr_2O_3 crystals

Table 1. EPR linewidth ratio, powder XRD data, TEM, fine structure and anisotropic fields of Cr_2O_3 doped silica glass.

Cr_2O_3:SiO_2 glass (mol%)	Calcination temperature (°C)	$\left(\frac{\Delta H_{pp}^{LNT}}{\Delta H_{pp}^{RT}}\right)$	$I_r = \frac{I^{LNT}}{I^{RT}}$	Crystallinity and Cr_2O_3 particle size (from powder XRD)	Cr_2O_3 particle size (from TEM)	Fine structure field (H_{fs}) (T)	Magnetic anisotropy field (H_a) at LNT (T)
1	800	1.9	—	Amorphous	—	—	—
(Cr1)	1000	6.3	62	Predominantly amorphous	—	—	—
10	800	3.3	19	Crystalline; 9 nm	7–10 nm	3.25	4.96
(Cr10)	1000	6.3	33	Crystalline; 11 nm	10–15 nm	3.25	7.40
	1200	8.9	346	Crystalline; 34 nm	>30 nm	2.94	8.30

progressively grow in intensity with increasing calcination temperatures. The x-ray diffraction lines of Cr10 samples calcined at 800 and 1000 °C due to Cr_2O_3 crystals exhibit significant line broadening, indicating that the crystal sizes are probably in the nanometre range. By taking consideration of the line [104] having maximum intensity, and applying the well-known Scherrer's equation [20], the sizes of chromium oxide crystals are estimated from the integral breadth of the peak (table 1). It is thus seen that the sizes of Cr_2O_3 crystals embedded in the silica glass fall in the nanometre range and become larger at higher calcined temperatures. In the XRD of 1200 °C calcined sample, the [200] line, being characteristic of CrO_3 crystals ($2\theta = 21.7°$), can be identified. This is a rather interesting finding in view of the fact that the unsupported bulk CrO_3 is not a stable compound at higher temperatures [21]. However, very recent thermogravimeric differential thermal analysis (DTA) and mass spectroscopic studies carried out up to 1000 °C [22] have revealed that Cr(VI) oxo-species are more stable when supported on a silica surface than CrO_3 alone, and so our observation of the presence of the CrO_3 compound at 1200 °C is vindicated.

3.2. TEM

TEM confirms the presence of Cr_2O_3 nanocrystals in the Cr10 glass specimens calcined at 800, 1000 and 1200 °C, sizes being greater for the samples calcined at higher temperatures (figure 2(i)). Spots are clearly visible in the electron diffraction photographs of samples calcined at 1200 °C, confirming that the Cr_2O_3 nanomaterials are crystalline (figure 2(ii)).

3.3. Absorption spectra

(a) IR absorption spectra (figure 3). Salient IR spectral features of silica gel–glasses doped with various chromium concentrations and calcined at various temperatures (calcination temperature denoted by T_{calc}) are the following:

(i) The involvement of a polycondensation process in the gel samples is supported by the behaviour of the IR band at ∼950 cm^{-1} (gel samples A, C, G), associated with the stretching mode Si–OH typical of gel structure [23]. This band is either very weak or totally absent for both doped and undoped silica glass samples calcined at various temperatures (samples B, D, E, F, H, I). It is thus evident that the gel-to-glass transformation is practically complete at 800 °C.

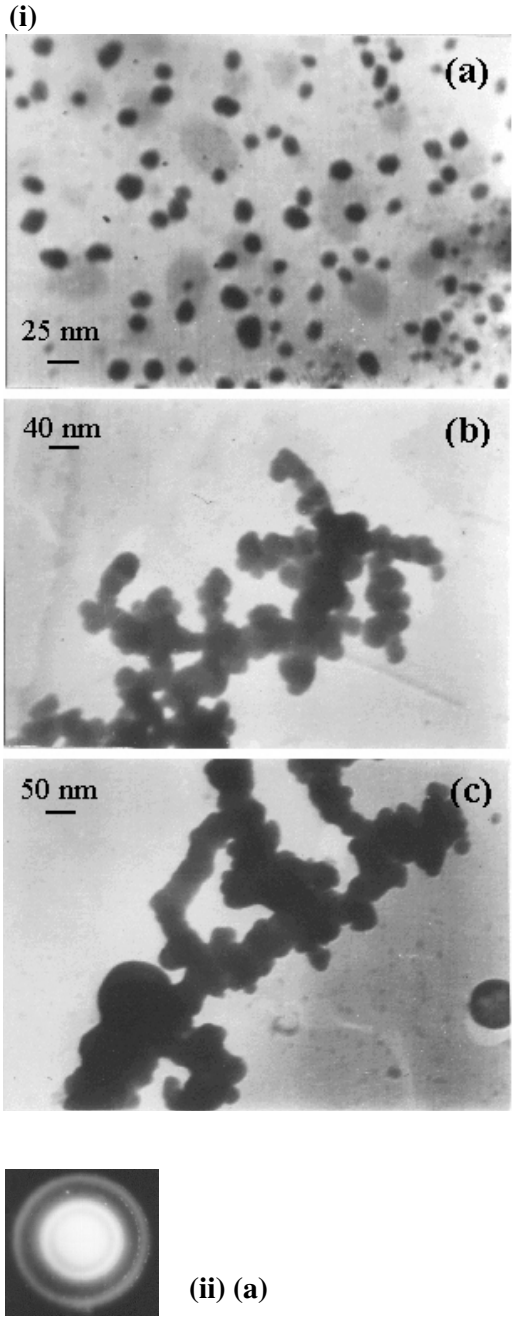

Figure 2. (i) Electron micrographs of Cr10 silica glass calcined at (a) 800 °C, (b) 1000 °C and (c) 1200 °C. (ii) Electron diffraction photograph of Cr10 silica glass calcined at 800 °C.

(ii) The bands at ∼1220 and ∼1100 cm^{-1} are associated with the LO mode and TO mode of the Si–O–Si asymmetric bond stretching vibration respectively [24], while the band at 800 cm^{-1} has been assigned to Si–O–Si symmetric bond stretching vibration and also to

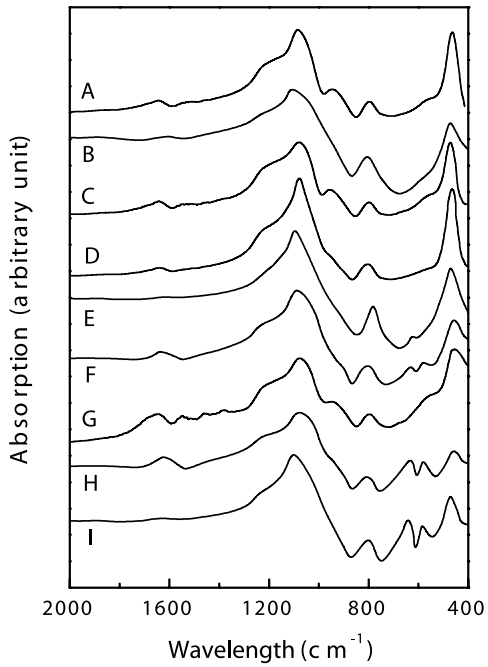

Figure 3. IR absorption spectra of Cr-doped silica glass at different doping concentrations: (A) pure gel dried at 40 °C, (B) pure glass calcined at 800 °C, (C) Cr1 gel dried at 40 °C, (D) Cr1 glass calcined at 800 °C, (E) Cr1 glass calcined at 1000 °C, (F) Cr5 glass calcined at 800 °C, (G) Cr10 gel dried at 40 °C, (H) Cr10 glass calcined at 800 °C, (I) Cr10 glass calcined at 1200 °C.

vibrational modes of the ring structure of SiO_4 tetrahedra. The band at ∼460 cm^{-1} is associated with a network of Si–O–Si bond bending vibration [25]. It is significant to note that the intensities of all these IR bands increase with increasing calcination temperature.

(iii) IR lines of Cr-doped silica glass obtained at ∼625 cm^{-1} (sample E), ∼630, ∼577 cm^{-1} (samples F, H) and ∼635, ∼579 cm^{-1} (sample I) are absent in IR spectra of pure silica glass (sample B) and have been identified to arise from Cr_2O_3 crystals present in these glasses [26]. This is consistent with powder XRD findings.

(b) Optical absorption spectra. Optical absorption spectra could only be recorded for Cr1 monolithic silica gel–glass (figure 4). Other silica glass samples having higher Cr dopant concentrations are opaque to the optical range used. The absorption peaks of RT dried gel observed at ∼420 nm (24 000 cm^{-1}) and ∼585 nm (17 000 cm^{-1}) may be assigned to $^4A_2(F) \rightarrow {}^4T_1(F)$ and $^4A_2(F) \rightarrow {}^4T_2(F)$ crystal field transitions respectively (figure 5(a)), similar to those observed in chrome alum crystal where each Cr^{3+} ion is octahedrally coordinated to six H_2O ligands [27, 28]. Thus Cr^{3+} ions in the silica glass are in the octahedral environment of O^- ions. The charge transfer band around 350 nm (∼30 000 cm^{-1}) and the absorption peak 867 nm (∼11 534 cm^{-1}) are shifted towards longer wavelength (corresponding to $10Dq$ shift) in the case of gel calcined at 500 °C. The shift of the charge transfer band implies that some of the Cr^{3+} ions are transformed to higher valence states. The situation is similar for the sample calcined at 800 °C. However, additionally two bands appear: one is broad, extending from 1350 nm (7407 cm^{-1}) to 1550 nm (6450 cm^{-1}), and the other is comparatively sharper, peaking at ∼1916 nm (5220 cm^{-1}). Analysis of the broad band further

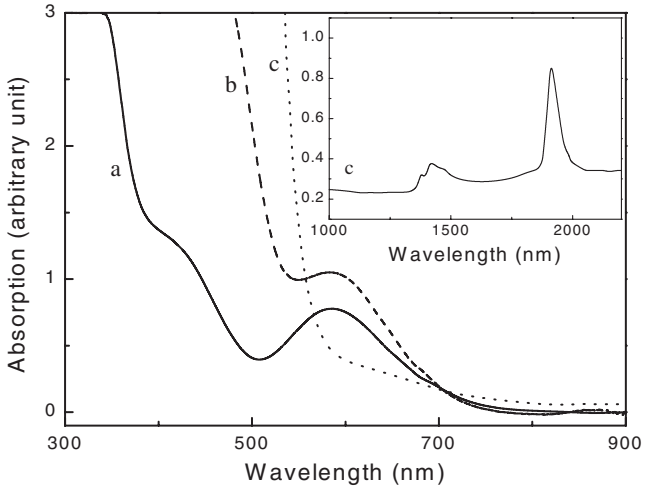

Figure 4. Optical absorption spectra of (a) Cr1 silica gel, room temperature dried, (b) Cr1 silica glass calcined at 500 °C and (c) Cr1 silica glass calcined at 800 °C.

reveals that it is actually composed of three Lorentzian lines centred at 1379 nm (7250 cm^{-1}), 1420 nm (7040 cm^{-1}) and 1475 nm (6780 cm^{-1}). These lines have been assigned to isolated Cr^{5+} ions having tetragonally distorted tetrahedral oxygen coordination with D_{2d} symmetry. The presence of narrow lines in the EPR spectrum has favoured the above assignment. The proposed ligand field energy scheme is shown in figure 5(b). Thus the annealing process brings out changes in the valency of the chromium dopant ions in an oxidative way. The ligand field bands will be further discussed in connection with the EPR spectral findings presented in the next section. The origin of the sharp peak at 5220 cm^{-1} is not clear to us. This requires further investigation for Cr1 samples calcined at various temperatures in the 500–800 °C range. It is relevant to mention here that Cr1 samples calcined at 900 °C and above are opaque, and so optical spectra cannot be recorded.

3.4. EPR spectra

X-band EPR spectra of Cr1, Cr5 and Cr10 (figures 6(a) and (b)) silica glasses calcined at 500, 700, 800, 900, 1000 and 1200 °C were recorded at RT and LNT temperatures. Each spectrum of Cr-doped silica glasses calcined at various temperatures is a broad line (type-I) with a narrow line (type-II) superimposed on it.

3.4.1. Type-I line. First derivative linewidth (ΔH_{pp}) versus calcined temperature curves for Cr1, Cr5 and Cr10 glass samples at both room and LN_2 temperatures are shown in figure 7 (see also table 2). For Cr10 glass samples the resonance line ($g \approx 1.97$) has ΔH_{pp} in the range 47–88 mT at RT. ΔH_{pp} at first increases with increasing calcination temperature, reaching a maximum at 900 °C and then it monotonically decreases. The interplay of dipolar broadening and exchange narrowing may be responsible for such linewidth behaviour. It might be that above 900 °C the exchange interaction plays a bigger role and the linewidth decreases. Unlike the RT spectrum, the LNT spectrum shows a spectacular rise in linewidth which falls in the range 140–570 mT, and there is not any perceptible resonance line shift. Thus the g-value obtained at LNT is the same as at RT, i.e., $g \approx 1.97$. This is also identical with the value of g

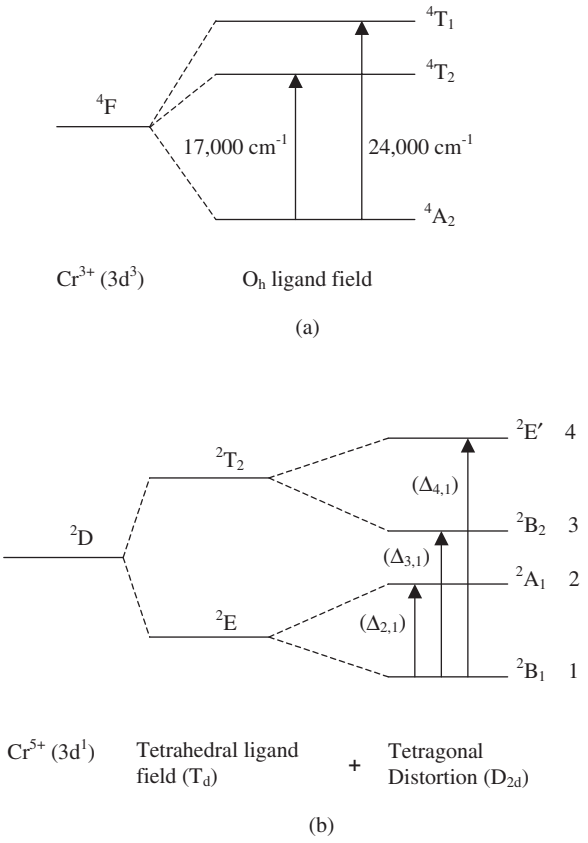

Figure 5. Splitting pattern of ligand field states of (a) Cr^{3+} ion under octahedral (O_h) ligand field, (b) Cr^{5+} ion under tetragonally distorted tetrahedral (D_{2d}) ligand field. 6780 cm^{-1} ($\Delta_{2,1}$), 7040 cm^{-1} ($\Delta_{3,1}$), 7250 cm^{-1} ($\Delta_{4,1}$).

obtained in the case of individual isolated Cr^{3+} ions, e.g. Cr^{3+} ions in phosphate glass [29]. Cr5 glass samples calcined at various temperatures depict similar characteristic EPR spectra at the same value of $g \approx 1.97$, and the ΔH_{pp}s are in the range 34–102 mT at RT and 23–520 mT at LNT. Cr1 glasses calcined at various temperatures (500–1000 °C) also exhibit type-I EPR spectra with $g \approx 1.96$ and ΔH_{pp}s in the range 38–76 mT at RT and 50–480 mT at LNT (figure 7). In view of the powder XRD findings, the broad line has been assigned to nanosized Cr_2O_3 particles. The broad line cannot have its origin in exchange coupled pairs of Cr^{3+} ion. EPR studies on exchange coupled Cr^{3+} pairs in emerald, i.e. Cr^{3+}-doped beryllium aluminium silicate [30] have shown a number of resonance lines arising from three types of Cr^{3+} pairs but ΔH_{pp}s of these lines are of the order of 5 mT, much less than those that have actually been observed.

In table 1, the derivative linewidth ratio $\left(\frac{\Delta H_{pp}^{LNT}}{\Delta H_{pp}^{RT}}\right)$ together with powder XRD data regarding the crystallinity and sizes of the nanocrystals have been shown for two dopant Cr_2O_3 concentrations in silica glass (Cr1 and Cr10). Although Cr1 silica glass samples calcined at 800 and 1000 °C are shown to contain amorphous Cr_2O_3 clusters, in sharp contrast with the corresponding Cr10 silica glass samples which contain Cr_2O_3 nanocrystals, the derivative linewidth ratios of Cr1 and Cr10 samples calcined at 1000 °C are surprisingly the same. On

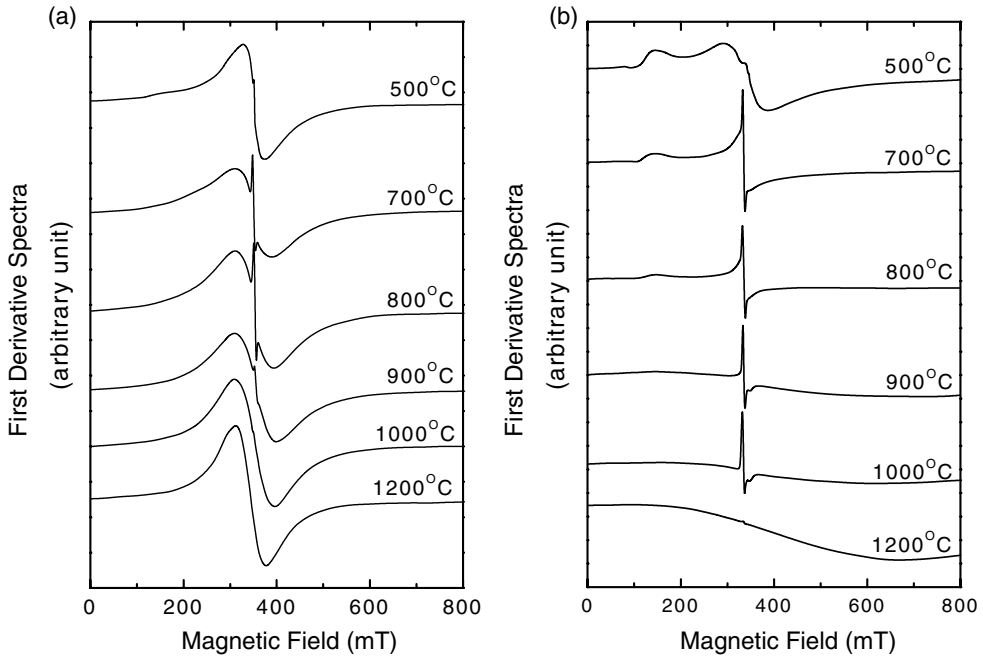

Figure 6. (a) RT EPR spectra of Cr10 silica glass calcined at various temperatures. (b) LNT EPR spectra of Cr10 silica glass calcined at various temperatures.

Table 2. First derivative linewidths (ΔH_{pp}) of Cr1, Cr5 and Cr10 glass samples calcined at various calcination temperatures and measured at RT and LNT.

Chromium-doped silica glass	Calcination temperature (°C)	First derivative linewidth ΔH_{pp} (mT)	
		RT	LNT
Cr1 ($g \approx 1.96$)	500	38	50
	700	40	52
	800	44	82
	900	50	400
	1000	76	480
Cr5 ($g \approx 1.97$)	500	34	23
	700	100	164
	800	102	300
	900	100	444
	1000	96	480
	1200	60	520
Cr10 ($g \approx 1.97$)	500	47	92
	700	76	140
	800	78	258
	900	88	460
	1000	78	480
	1200	64	570

the other hand, the linewidth ratios for these samples calcined at 800 °C are very different, being greater for Cr10 sample (3.3 against 1.9) (table 1). For Cr10 samples it is further seen

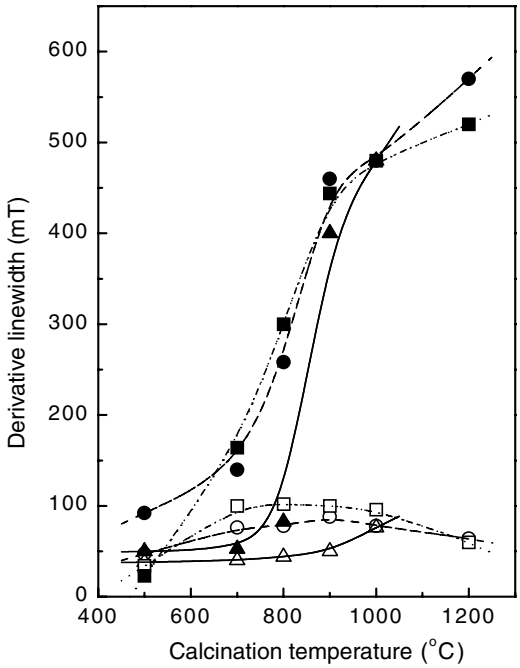

Figure 7. First derivative linewidth (ΔH_{pp}) of the broad EPR (type-I) line versus calcination temperature for Cr1, Cr5 and Cr10 silica glass samples. —△—: 1% Cr-RT; —▲—: 1% Cr-LNT; - □ -: 5% Cr-RT; - ■ -: 5% Cr-LNT; ···○···: 10% Cr-RT; ···●···: 10% Cr-LNT.

that the derivative linewidth ratio is much larger for larger size Cr_2O_3 nanocrystals. The intensities of the EPR lines are also calculated using the approximate formula $I = A \times \Delta H_{pp}^2$ (A is the amplitude of the first derivative signal). For Cr10 glass, the relative EPR intensity I_r, i.e., $\frac{I^{LNT}}{I^{RT}}$, is found to be much larger, and it is largest (346.0) at 1200 °C, the highest calcination temperature employed in the present experiment (table 1). Such an enormous rise in EPR line intensities in going from RT to LNT suggests that the exchange coupling in these magnetic nanocrystals is ferromagnetic type and that the ferromagnetism is of greater magnitude for larger size nanocrystals. I_r has been estimated only in the case of Cr1 sample calcined at 1000 °C. Interestingly enough, I_r is found to be almost double that obtained for Cr10 sample calcined at the same temperature of 1000 °C (62 against 32), which implies that amorphous Cr_2O_3 nanoparticles in Cr1 sample are more strongly ferromagnetic than the Cr_2O_3 nanocrystals in Cr10 sample, both being calcined at 1000 °C. For Cr10 glass the relative intensity I_R at LNT (with respect to the 500 °C calcined sample intensity) versus calcination temperature (T_{calci}) has been plotted in figure 8. The curve, starting from 800 °C, shows a fast continuous increase in I_R up to 1200 °C, the highest calcination temperature employed in the present experiment. This is consistent with the fact that the collapse of pores in the silica glass starts at ∼700 °C and is nearly completed at ∼800 °C [17], leading to the formation of Cr_2O_3 nanoparticles.

We have also attempted an explanation of the large variation of linewidth in going from RT to LNT in the case of Cr10 samples containing Cr_2O_3 nanocrystals, on the basis of the well-known Anderson–Weiss expression for linewidth [31]:

$$\Delta H_{1/2} = (\tfrac{10}{3} H_p^2 + H_{fs}^2 + H_a^2)/H_{ex} \tag{1}$$

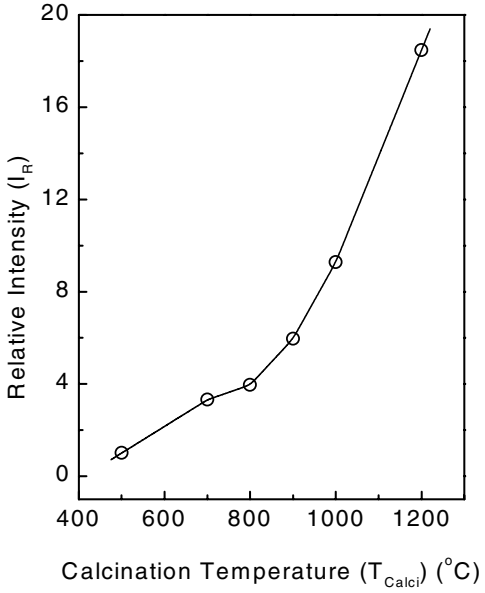

Figure 8. Relative EPR intensity (I_R) with reference to that at 500 °C versus calcination temperature curve for Cr10 silica glass at LNT.

where $\Delta H_{1/2}$ is the absorption linewidth at half maximum; H_p is the dipolar field, given by

$$H_p^2 = 5.1[g\beta N\rho/M]^2 S(S+1). \tag{2}$$

H_{fs} is a contribution from fine-structure crystalline field and H_a is the magnetic anisotropy field present only in the non-paramagnetic state which may be superparamagnetic, antiferromagnetic, ferromagnetic or ferrimagnetic. H_{ex} is the exchange field, given by

$$[2.83S(S+1)]^{1/2}\frac{J}{g\beta} \tag{3}$$

where g is the splitting factor, equal to 1.97 (experimentally obtained), N is Avagadro's number; ρ, M are density and molecular weight of Cr_2O_3 respectively, $S = 3/2$ for Cr(III) ion, and J is the isotropic exchange integral. The value of J has been taken to be that obtained for bulk Cr_2O_3 crystal, which is 68.63 cm^{-1} [32]. Inter-nanocrystal interaction has not been considered. With the help of equation (3) and using $J = 68.63$ cm^{-1}, H_{ex} is estimated to be about 245 T. Using equation (1), from RT linewidth data H_{fs} is estimated when $H_a \approx 0$. Then, using the same expression (1), H_a is estimated from LNT linewidths. Values of H_a are included in table 1. The values of H_a so obtained are quite large, indicating that Cr_2O_3 nanocrystals possess large magnetic anisotropy fields (H_a) of varying amounts at LNT depending on particle sizes.

It is worthwhile comparing here the above results for Cr_2O_3 nanocrystals with those obtained for bulk Cr_2O_3 crystal from magnetic susceptibility and EPR studies [33]. The bulk crystal becomes antiferromagnetic (AF) below 307 K (T_N), and its EPR absorption line shows large shift towards lower magnetic field and becomes very broad as well, to the limit of being almost untraceable while approaching T_N from above. Thus, unlike antiferromagnetic Cr_2O_3 bulk crystals, Cr_2O_3 nanocrystals at 77 K show ferromagnetic character and are associated with large magnetic anisotropy fields as obtained from EPR linewidth analysis. All these facts suggest that Cr_2O_3 nanocrystals possibly have single domain ferromagnetic structure [6].

In this connection it is relevant to refer to the important findings of Raman spectroscopic and other studies (including measurements of pore size, density and specific surface area) by Krol and Lierop [19] on the densification of undoped SiO_2 gel as a function of heat treatment between 120 and 900 °C. Their studies have revealed that the average pore size increases abruptly from 1.0 nm at 700 °C to 2.3 nm at 800 °C, while in the same temperature interval the specific surface area decreases from 550 to 160 $m^2\ g^{-1}$ and the pore volume/g decreases from 0.19 to 0.12 $cm^3\ g^{-1}$. Smaller pores collapse at lower temperatures, because of their higher surface energy. The surface energy is also influenced by the hydroxyl coverage of the gel, and is higher for a siloxane surface than for a hydroxyl surface. With increasing temperature ≡Si–OH groups condense to ≡Si–O–Si≡ bonds, thus increasing the surface energy and enhancing pore collapse. At 800 °C, a significant number of small pores collapse and the rest of the pores join to form larger pores. In this calcined glass having very high magnetic dilution, agglomeration of individual Cr_2O_3 ions entrapped in small pores into nanoparticles takes place as a result of pore collapse. At still higher temperature, i.e., 1000 °C, collapse of larger pores also takes place, similar to that which has been observed in an undoped sample, indicated by the rapid fall of pore volume/g from 0.12 to 0.026 $cm^3\ g^{-1}$ in going from 800 to 900 °C. Raman spectral studies have also indicated that at 900 °C the surface Si–OH groups have completely disappeared, condensing to ≡Si–O–Si≡ bonds and increasing the surface energy, leading to almost complete annihilation of pores. Thus it is possible at the highest temperature, i.e., 1200 °C in the present case, Cr_2O_3 nanoparticles grow to maximum size. The observed enhancement of EPR linewidth as well as the somewhat dissimilar nature of the thermal dependence of the linewidth of Cr-doped silica glass (table 2, figures 6(a) and (b)) indicates that the EPR behaviours of these nanoparticles depend very much on their sizes.

3.4.2. Type-II line. Computer simulation reveals that the type-II narrow resonance line of Cr10 sample has a slightly anisotropic g-value, $g_\perp > g_\parallel$ ($g_\parallel = 1.955$, $g_\perp = 1.976$) and anisotropic linewidth ($\Delta H_{pp}^{\parallel} = 1.9$ mT, $\Delta H_{pp}^{\perp} = 1.2$ mT). The type-II line has been assigned to isolated Cr^{5+} ions under tetragonally distorted tetrahedral environments of oxygen ligands. The justification for such an assignment is as follows. When our optical findings described in the previous section 3.3(b) (figure 5(b)) are considered in conjunction with anisotropic g-values, it follows that the excited ligand field states $^2A_1$, $^2B_2$, ^2E lie at 6780, 7040 and 7250 cm^{-1} respectively above the ground state ($^2B_1$). The first excited state $^2A_1$, not being spin–orbit coupled to the ground state $^2B_1$, the Cr^{5+} ion is expected to have a large spin–lattice relaxation time, giving rise to the observed narrow line.

Ligand field analysis. The expressions for the spin Hamiltonian parameters $g_\parallel$, $g_\perp$ applicable for a Cr^{5+} ($3d^1$) ion under a tetragonally distorted tetrahedral ligand field of O^- ions having D_{2d} symmetry with $^2B_1$ as the ground state can be easily derived using a perturbation procedure up to second order, and are given below:

$$g_\parallel = 2\left[1 - \frac{4k_{13}R_{13}\lambda}{\Delta_{3,1}}\right] \qquad \text{and} \qquad g_\perp = 2\left[1 - \frac{k_{14}R_{14}\lambda}{\Delta_{4,1}}\right], \tag{4}$$

where λ is the spin–orbit coupling constant of the Cr^{5+} ion; $\Delta_{3,1}$ and $\Delta_{4,1}$ are the ligand field separations as indicated in figure 5(b); k_{ij} and R_{ij} are orbital reduction and spin–orbit reduction factors respectively, and they take care of covalent metal–ligand interactions in the manner of Stevens [34], Owen [35] and Tinkhan [36]. On the simplifying assumption $k_{ij} = R_{ij}$ and taking $\lambda = +380\ cm^{-1}$ for the free Cr^{5+} ion, $\Delta_{3,1} = 7040\ cm^{-1}$, $\Delta_{4,1} = 7250\ cm^{-1}$ (obtained from optical spectra), $g_\parallel = 1.955$, and $g_\perp = 1.976$ (obtained from EPR analysis), the covalency parameters are estimated to be $R_{13} = 0.322$ and $R_{14} = 0.478$. This result shows

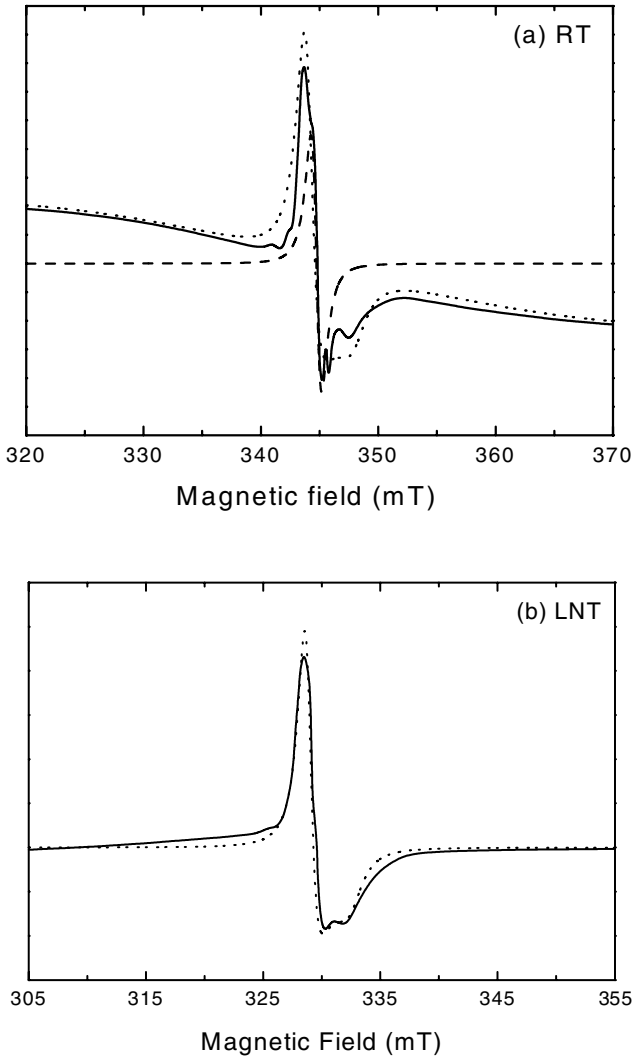

Figure 9. EPR spectra of Cr10 glass calcined at 800 °C. (a) At room temperature: (i) $g_{\parallel} = 1.955$, $g_{\perp} = 1.976$, $\Delta H_{pp}^{\parallel} = 1.9$ mT, $\Delta H_{pp}^{\perp} = 1.2$ mT; (ii) $g_{\parallel} = g_{\perp} = 1.973$, $\Delta H_{pp} = 0.9$ mT, $\nu = 9.515$ GHz; (iii) $g_{\parallel} = g_{\perp} = 1.969$, $\Delta H_{pp} = 70$ mT; ·····: (i) + (ii); - - - -: (ii); ——: experimental. (b) At LNT temperature: $g_{\parallel} = 1.955$, $g_{\perp} = 1.976$, $\Delta H_{\parallel} = 1.7$ mT, $\Delta H_{\perp} = 1.0$ mT $\nu = 9.094$ GHz; ·····: theoretical; ——: experimental.

profound covalent character of the Cr^{5+}–O bond in the Cr^{5+} tetrahedral complex embedded in the silica glass matrix.

For the glass samples calcined at 700, 800 and 900 °C, computer analysis has further revealed the presence of another sharp isotropic line ($g = 1.973$) having Lorentzian lineshape and $\Delta H_{pp} = 0.9$ mT (figure 9). The isotropic line probably arises from freely rotating individual Cr^{5+} ions having tetrahedral oxygen coordination situated at some other sites in the silica glass matrix. The isotropic line, however, disappears at LNT. It is possible that the rotation of the Cr^{5+} complex ion ceases at LNT, giving rise to an anisotropic spectrum which merges with the anisotropic narrow line spectrum already present at RT. The narrow spectrum due to Cr^{5+} ions gradually becomes less intense in samples treated at higher calcination

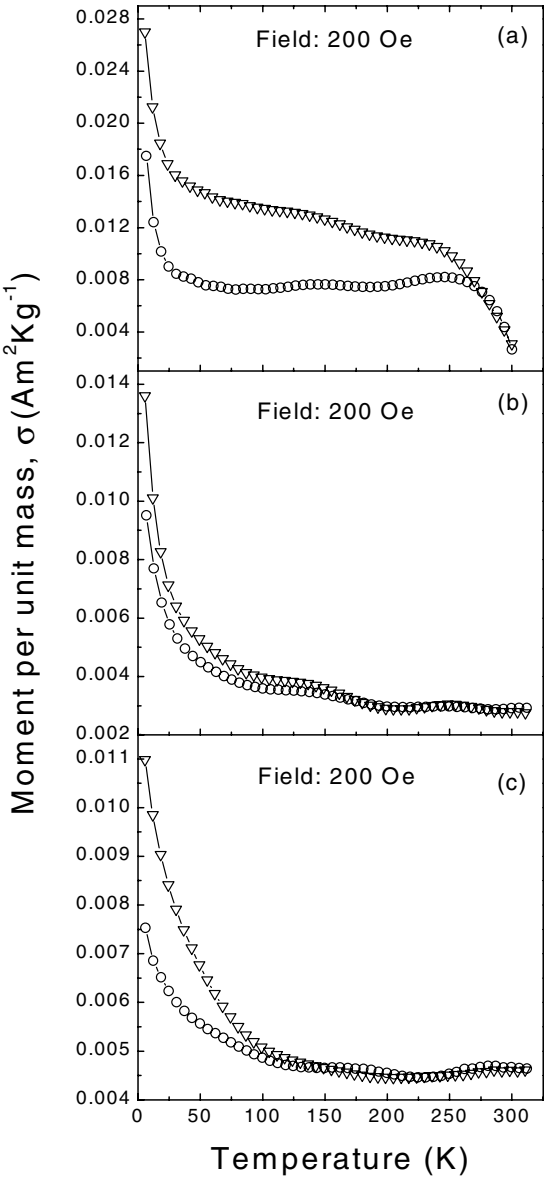

Figure 10. Temperature dependence of magnetization (ZFC and FC) of Cr10 glass calcined at (a) 800 °C, (b) 1000 °C and (c) 1200 °C. O: ZFC; △: FC.

temperature and nearly vanishes in samples calcined at 1200 °C (figure 6(b)). It is most likely that the conversion of Cr^{5+} ions to Cr^{6+} ions by oxidation is facilitated at higher calcination temperature. Confirmatory evidence comes from powder XRD (figure 1) which reveals the occurrence of CrO_3 nanocrystals in Cr10 samples calcined at 1200 °C. For 500, 700 and 800 °C samples, another resonance line at $g_{\text{eff}} \cong 4.51$ is additionally observed which may arise from some isolated Cr^{3+} ions trapped at some sites having highly distorted octahedral oxygen environments.

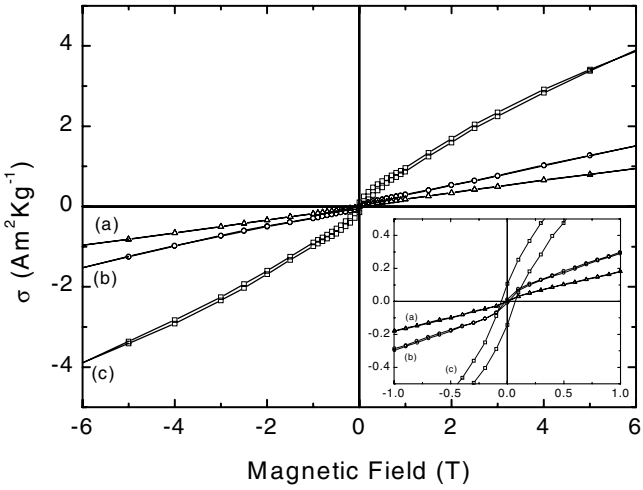

Figure 11. Hysteresis loops of calcined (calcination temperature: 800 °C) Cr10 silica glass sample recorded at (a) 300 K (△); (b) 100 K (○); and (c) 5 K (□). In the inset, the region close to the coercive field value is highlighted.

3.5. ZFC, FC and hysteresis

ZFC and FC magnetization curves for Cr10 samples calcined at 800, 1000 and 1200 °C as a function of temperature in presence of applied magnetic field of 200 Oe are displayed in figure 10.

For the sample calcined at 800 °C, the magnetic moments in the ZFC and FC curves, with the increase of temperature starting from 5 K, at first show a continuous decrement. Above 50 K, the ZFC curve exhibits nearly a plateau region and then on reaching 200 K shows a slow monotonic increase terminating in a broad peak at ≈250 K. The magnetization again decreases on increasing the temperature beyond 250 K. At ≈275 K, both the ZFC and FC curves converge and show the same decreasing trend with further increase in temperature. Such behaviour is akin to superparamagnetism [37, 38] and the temperature corresponding to the maximum in the ZFC curve most likely is the blocking temperature (T_B), typical of this measurement technique. Since nanoparticle size distribution is present, a spread in the blocking temperature may be rightly assumed, leading to the observed broad peak in the ZFC curve. In the low temperature region (<25 K) there is a very steep increase in the magnetization as is evident from both the ZFC and FC curves (figure 10(a)), and it is apparent that the nanoparticles assume ferromagnetic order. Figure 11 shows three magnetic hysteresis curves obtained at 300 K (a), 100 K (b) and 5 K (c) in the magnetic field range of ±6 T. The magnetization loop (zero area) obtained at 300 K displays characteristics of superparamagnetism. Below T_B, i.e., at temperatures 100 and 5 K, hysteretic behaviours are observed. The 100 K loop shows a small remanence. The hysteresis is more pronounced at 5 K and brings out clearly the ferromagnetic behaviour of the sample.

Figures 10(b) and (c) depict ZFC and FC magnetization curves for Cr10 samples calcined at 1000 and 1200 °C recorded in the 5–310 K temperature range. In these two samples, a steep rise in the magnetization (both ZFC and FC) occurs below 50 and 75 K respectively, indicating the emergence of ferromagnetic order. The two curves nearly coincide at higher temperatures (>100 K), and the same decreasing trend of the magnetic moments with increasing temperature is continued. Figures 12(i) and (ii) show the hysteresis loops of samples calcined at 1000 and 1200 °C respectively, and in each case measurements are carried out at two temperatures,

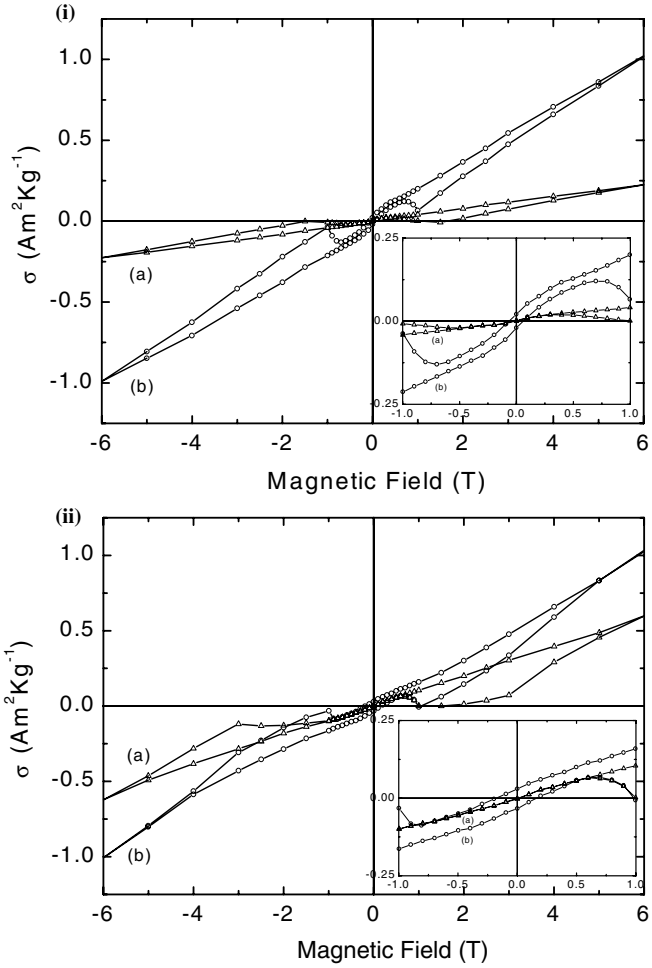

Figure 12. (i) Hysteresis loops of calcined (calcination temperature: 1000 °C) Cr10 silica glass sample recorded at (a) 300 K (△); (b) 5 K (○). (ii) Hysteresis loops of calcined (calcination temperature: 1200 °C) Cr10 silica glass sample recorded at 300 K (△); (b) 5 K (○). In the inset, the region close to the coercive field value is highlighted.

namely, 300 K (a) and 5 K (b). For the sample calcined at 1000 °C, the hysteresis graph at 300 K looks as if it is pinched, i.e., very much narrowed down in the ±1 T magnetic field range, whereas at 5 K it is more spaced. If we compare our results with the 800 °C calcined sample (figure 11), the 1000 °C calcined sample displays the presence of ferromagnetism even at 300 K, although it is apparent only in the presence of higher magnetic fields (>±1 T). Of course, ferromagnetism is more pronounced for this sample at 5 K. This is evident from the bulging of hysteresis loop near the central region (low field region), and also the magnetic moment/unit mass is many times enhanced compared to that at 300 K. The above trend is more prominently displayed in the sample calcined at 1200 °C (figures 10(c) and 12(ii)). However, it is to be noted that the magnetic moment per unit mass for Cr_2O_3 nanoparticles at the lowest temperature of our measurement, i.e., 5 K in Cr10 samples calcined at 800 °C, is much more than that of larger sized Cr_2O_3 nanoparticles of Cr10 samples calcined at 1000 and 1200 °C. This may be due to the fact that some conversion of Cr_2O_3 samples to diamagnetic CrO_3

particles take place at higher temperatures, the correction for which has not been taken into account in the magnetic moment per unit mass calculation.

4. Conclusions

(i) It has been possible to satisfactorily synthesize nanocrystalline Cr_2O_3 particles in silica glass matrices by a sol–gel method at calcination temperatures 800 °C and above. The crystallinity of the particles and their sizes have been determined by XRD and TEM. Cr_2O_3 nanocrystals are obtained in larger sizes at higher calcination temperatures. Some IR bands which are characteristic of Cr_2O_3 particles have been identified.

(ii) Formation of isolated Cr^{5+} ions having distorted tetrahedral oxygen coordination in Cr-doped SiO_2 glass samples calcined at 500 °C has been established by EPR and optical studies. It is further seen that Cr^{5+} ions are gradually oxidized to Cr^{6+} ions with the increase of calcination temperature, and conversion is nearly complete at 1200 °C calcination temperature.

(iii) From XRD studies, the presence of CrO_3 nanocrystals in Cr10:SiO_2 glass calcined at 1200 °C has been confirmed. These crystals, being diamagnetic, are not amenable to EPR studies.

(iv) EPR features (g and linewidth) of nanocrystalline Cr_2O_3 particles observed at room and LN temperatures are quite distinct from those of bulk Cr_2O_3 crystals, and are possibly manifestations of superparamagnetism/ferromagnetism in these nanocrystals. Investigations of the thermal dependence of magnetization (ZFC and FC) and magnetic hysteresis of Cr10:SiO_2 glass calcined at 800, 1000 and 1200 °C in the 5–300 K temperature range have provided ample confirmatory evidence. These studies have clearly shown the presence of superparamagnetic behaviour for the sample calcined at 800 °C, the ferromagnetic effect being apparent at low temperature ($\leqslant$100 K). Ferromagnetic effects are more prominently displayed in the samples calcined at 1000 and 1200 °C, even observable at 300 K in the magnetic hysteresis curve.

Acknowledgments

The authors are indebted to the referees of this paper for some valuable suggestions and advice in improving the quality of the paper. One of the authors (S Bhattacharya) gratefully acknowledges financial support from Academi of Finland, Grant No. 204844.

References

[1] Douglass D C, Cox A J, Bucher J P and Bloomfield L A 1993 *Phys. Rev.* B **47** 12874
[2] Ganteför G and Eberhardt W 1996 *Phys. Rev. Lett.* **76** 4975
[3] Reddy B V, Khanna S N and Dunlap B I 1993 *Phys. Rev. Lett.* **70** 3323
[4] Bertsch G F, Onishi N and Yabana K 1995 *Z. Phys.* D **34** 213
[5] Reddy B V and Khanna S N 1999 *Phys. Rev. Lett.* **83** 3170
[6] Dormann J L, Fiorani D and Tronc E 1997 *Magnetic Relaxation in Fine-Particle Systems* (*Advances in Chemical Physics* vol 98) ed I Prigogine and S A Rice (New York: Wiley) p 283
[7] Hansen M F, Bødker F, Mørup S, Lefmann K, Clausen K N and Lindgård P-A 1997 *Phys. Rev. Lett.* **79** 4910
[8] Chen Q and Zhang Z J 1998 *Appl. Phys. Lett.* **73** 3156
[9] Zysler R D, Fiorani D and Testa A M 2001 *J. Magn. Magn. Mater.* **224** 5
[10] Berger R, Kliava J, Bissey J C and Baïetto V 1998 *J. Phys.: Condens. Matter* **10** 8559
[11] Uhm Y R, Kim W W, Kim S J, Kim C S and Rhee C K 2003 *J. Appl. Phys.* **93** 7196
[12] Kodama R H, Makhlouf S A and Berkowitz A E 1997 *Phys. Rev. Lett.* **79** 1393

[13] Punnoose A, Magnone H, Seehra M S and Bonevich J 2001 *Phys. Rev.* B **64** 174420
[14] Balachandran U, Liao X Y, Askew T R and Siegel R W 1995 *Nanostruct. Mater.* **5** 505
[15] McGuire T R, Scott E J and Grannis F H 1956 *Phys. Rev.* **102** 1000
[16] Vollath D, Szabó D V and Willis J O 1996 *Mater. Lett.* **29** 271
[17] Nogami M and Moriya Y 1980 *J. Non-Cryst. Solids* **37** 191
[18] Sakka S and Kamiya K 1982 *J. Non-Cryst. Solids* **48** 31
[19] Krol D M and van Lierop J G 1984 *J. Non-Cryst. Solids* **63** 131
[20] Klug H P and Alexander L E 1974 *X-Ray Diffraction Procedure for Polycrystalline and Amorphous Materials* 2nd edn (New York: Wiley) p 661
[21] Chamberland B L 1997 *Solid State Mater. Sci.* **7** 1
[22] Jóźwiak W K, Ignaczak W, Dominiak D and Maniecki T P 2004 *Appl. Catal.* A **258** 33
[23] Decottignies M, Phalippou J and Zarzycki J 1978 *J. Mater. Sci.* **13** 2605
[24] Bertoluzza A, Fagnano C and Morelli M A 1982 *J. Non-Cryst. Solids* **48** 117
[25] Simon I 1960 *Modern Aspect of the Vitreous State* vol 1, ed J D Mackenzie (London: Butterworths Scientific Publication Ltd)
[26] Nyquist R A and Kagel R O 1971 *Infrared Spectra of Inorganic Compounds* (New York: Academic) p 216
[27] Bates T 1962 Ligand-field theory and absorption spectra of the transition metal ions *Modern Aspects of the Vitreous State* vol 2, ed J D Mackenzie (London: Butterworths Scientific Publications Ltd) p 228
[28] Tanaka K and Kamiya K 1991 *J. Mater. Sci. Lett.* **10** 1095
[29] Landry R J, Fournier J T and Young C G 1967 *J. Chem. Phys.* **46** 1285
[30] Edger A and Hutton D R 1978 *J. Phys. C: Solid State Phys.* **11** 5051
[31] Anderson P W and Weiss P R 1953 *Rev. Mod. Phys.* **25** 269
[32] Foner S 1963 *Phys. Rev.* **130** 183
[33] Anufriev V G 1977 *Phys. Lett.* A **64** 139
[34] Stevens K W H 1951 *Proc. R. Soc.* A **205** 135
[35] Owen J 1955 *Proc. R. Soc.* A **227** 183
[36] Tinkham M 1956 *Proc. R. Soc.* A **236** 535
[37] Néel L 1949 *Ann. Geophys.* **5** 99
[38] Bean C P 1955 *J. Appl. Phys.* **26** 1381